Measurement of the Interaction Between a Rotor Tip Vortex and a Cylinder

S. G. Liou,* N. M. Komerath,† and H. M. McMahon‡
Georgia Institute of Technology, Atlanta, Georgia

The transient interaction between a cylinder and the trailing vortex from a rotor in forward flight is studied. Phase-averaged laser velocimetry and surface pressure measurements made with flush-mounted microphones are used to study the velocity and pressure variations during such an interaction. Vorticity contours constructed from the velocity measurements exhibit the presence of a secondary structure with vorticity opposite in sense to that of the primary tip vortex. This structure moves rapidly around the tip vortex from upstream to downstream. The pressure variations caused by the tip vortex on the surface of the cylinder are smooth as the vortex core passes by, and no evidence is found of fine structure inside the vortex core region. After vortex interaction, the secondary structure causes large variations in the surface pressure before being dissipated. Calculations using measured vortex strength and speed data indicate that the distortions and deflections of the vortex immediately prior to impingement on the surface differ significantly from those computed using two-dimensional potential flow concepts.

Nomenclature

Cp_u = unsteady pressure coefficient: difference between the instantaneous pressure and the local mean static pressure, normalized by the tunnel dynamic pressure
R = rotor radius
r = radial position along the rotor radius
U = velocity component along the tunnel axis, positive going downstream
U_∞ = freestream velocity
V = vertical velocity component, positive downward
X = distance parallel to the tunnel axis, origin is at the rotor hub center
Xb = distance parallel to the tunnel axis, measured from the nose of the cylinder
Yb = distance along the lateral direction from the cylinder axis
Zb = vertical distance from the cylinder axis, positive upwards
Z' = vertical distance from the top surface of the cylinder
$\Gamma(r)$ = radial distribution of bound circulation on the rotor blade
Ψ = azimuthal location of the 1/4-chord line of the reference rotor blade, zero at the trailing edge of the rotor disc
θ = azimuth angle going around the periphery of the cylinder, zero at the top
μ = advance ratio, ratio of freestream velocity to rotor tip speed
ϕ = age of the vortex cross section, in degrees of rotor azimuth, $\phi = \Psi - 180$

Introduction

VORTICES shed from lifting surfaces can cause strong effects on solid surfaces in their vicinity. The problem studied in this paper is the interaction of the tip vortex from a rotor blade with a curved surface. Blade tip vortices are the dominant features of the wake of a lifting rotor. In hover or low-speed flight, the airframe of a rotorcraft is immersed in the rotor wake (Fig. 1). The presence of the airframe significantly affects the behavior of these vortices, and thus their induced velocity field. Viscous effects near solid walls change the vortices, and perhaps cause the formation of other vortex structures. The vortex trajectories may be expected to be modified. Conversely, the vortices, being concentrated regions of high velocity and pressure gradients, must have drastic effects on the flow over the airframe. The locations on the airframe where such interactions occur, and the magnitude of their effects, cannot be predicted without first being able to model the behavior of the vortices in the vicinity of the airframe. Physical models of such interactions are needed to predict the aerodynamics and the forcing functions that dictate the dynamics of rotorcraft.

There are major differences between the straight vortex filaments that trail fixed-wing aircraft and the curved, approximately helical filaments that trail rotor systems. A curved vortex, according to potential flow theory, can induce velocities on itself. The structure of the vortex becomes very important in calculating induced velocities near the vortex. Also, there are strong axial velocity components inside the core of the vortex. In forward flight, the circulation on a rotor blade changes with rotor azimuth. Thus, the strength of any given part of the trailing vortex filament is a function of the rotor azimuth when that part left the blade. A further complication is the inboard vortex sheet. The radial distribution of bound circulation on a rotor blade typically shows a strong peak inboard of the blade tip. The radial derivative of the circulation thus changes sign at this station, and the inboard vortex sheet has a sign of vorticity that is opposite to that of the tip vortex. The outer portion of the vortex sheet rolls up into the dominant tip vortex. As the vortex nears the surface, the effects of the surface, as modeled by placing "image vortices" beneath the surface, would suggest that convection of the tip vortex would be retarded, and convection of the vortex sheet would be accelerated, so that the tip vortex and the vortex sheet would be separated. Measurements presented in Ref. 1 support this expectation.

Previous Work

Some of the previous efforts in this field are briefly summarized in Ref. 1. Stremel[2] computed the motion of a straight

Received Jan. 24, 1989; revision received July 17, 1989.

*Post-Doctoral Fellow, School of Aerospace Engineering. Member AIAA.
†Assistant Professor, School of Aerospace Engineering. Member AIAA.
‡Professor, School of Aerospace Engineering. Senior Member AIAA.

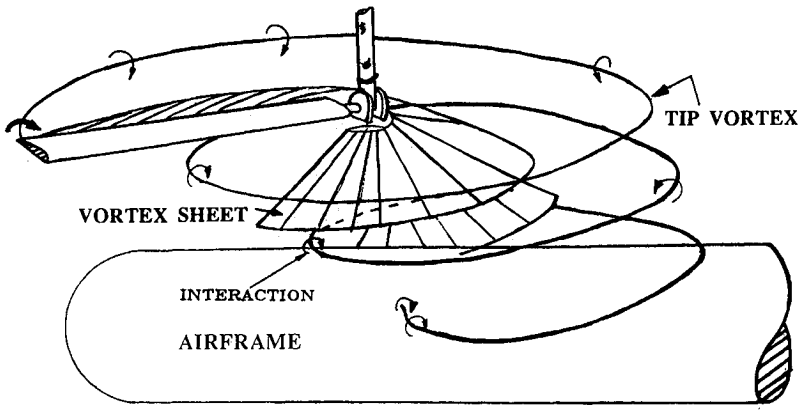

Fig. 1 The wake of a single-bladed rotor impinging on an airframe in low-speed forward flight.

vortex filament in a vortical wake as it approached a circular cylinder. Harvey and Perry[3] and Atiahs and Weihs[4] studied fixed-wing aircraft trailing vortices near the ground, and found that the boundary layer at the ground separated. A secondary vortex formed, which had a sense of rotation opposite to that of the trailing vortex. This caused the vortex trajectory to rise and its horizontal motion to decelerate. The trailing vortex trajectory also showed periodic oscillations which were attributed to an elliptical vortex core shape. Similar results were observed experimentally and analytically on a convected two-dimensional vortex and a vortex ring impacting on a wall by Doligalski and Walker[5] and Walker et al.[6] In the vortex ring interaction, unsteady separation developed in the boundary-layer flow in the form of a secondary ring attached to the wall. A period of rapid boundary-layer growth ensued, with strong viscous-inviscid interactions. The secondary vortex ring was ejected from the boundary layer and the primary ring then interacted with the secondary ring and rebounded from the wall.

Simons et al.[7] noticed that as the tip vortex from a rotor blade approached the rotor supporting pylon, it deformed and wrapped around the nose of the pylon. The vortex filament distorted, and the vortex core began to break up from both ends and spiral in a helix. As the vortex moved across the pylon, this spiral propagated outwards toward a similar spiral which was moving inwards from the edge of the vortex. Thus, within a very short distance, the vortex structure changed from a tightly rolled core to a diffuse, swirling flow. This process has similarities with the situation being studied in this paper. Recently, Bliss[8] has developed a method for analyzing close vortex-surface interactions, eliminating the need for dense paneling of the surface. He analytically simulates the force-free motion of the vortex filaments in close proximity to solid surfaces, and uses local solutions to accurately treat close filament-surface interactions.

Present Scope

This paper extends the work reported in Ref. 1. In particular, we have obtained quantitative measures of the validity of simple two-dimensional potential flow models for the interaction. The pressure variations at the surface during close vortex interaction are studied with higher temporal resolution, and are compared to the velocity variations immediately above. Also, a more extensive database has been obtained, and a clearer picture of the interaction has emerged. The vorticity field above the airframe is studied as the vortex approaches the surface in order to seek the origin and evolution of secondary structures.

Test Configuration

A relatively simple geometry is used. As shown in Fig. 2, a cylinder of 134 mm diam with a hemispherical nose is sting-mounted from the wind-tunnel floor. The hub centerline is located one rotor radius downstream of the cylinder nose. The cylinder is instrumented with static taps and microphone ports. A two-bladed rotor of radius 0.914 m is mounted from the tunnel ceiling. The NACA 0015 blades are rigidly fixed to the hub, untwisted, untapered and set at 10-deg pitch. The hub pivots about a pin through the rotor shaft, so that the blades are free to flap. This geometry results in the blade tips being heavily loaded so that the wake is dominated by strong tip vortices.

An electrical pulse generated once every shaft revolution when the blades are aligned along the cylinder axis serves to relate all data to the azimuthal location of the reference blade at the instant of data acquisition. The shaft speed was held at 2100 rpm. At an advance ratio of 0.1, the freestream velocity was 10 m/s. The rotor tip path plane had longitudinal and lateral flapping angles of 4.06 deg and 2.03 deg, respectively, under these conditions, with the cylinder axis placed $0{\cdot}3R$ below the rotor hub.

Pressure Measurements

All of the data reported here were phase-averaged, i.e., data arriving at the same phase of a periodic process were averaged to give the averages over many cycles of the process. This implies that non-periodic phenomena such as turbulence were filtered out. The validity of this was confirmed separately for each of the diagnostic techniques used.

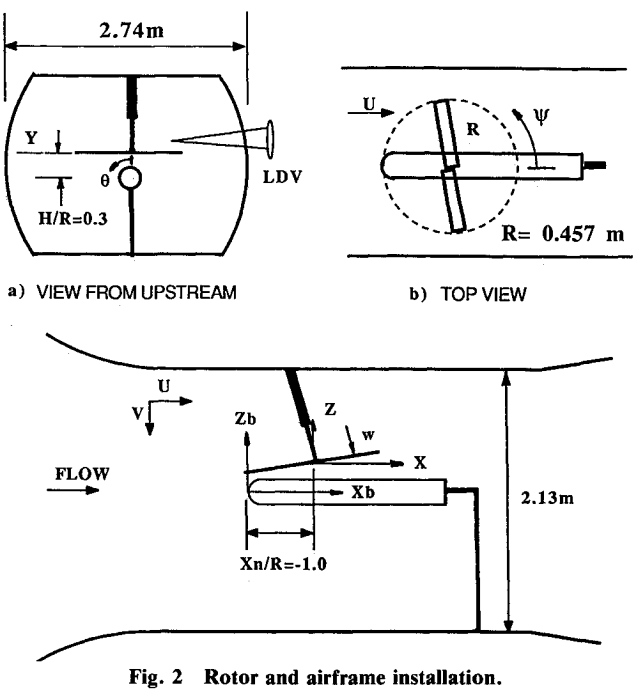

Fig. 2 Rotor and airframe installation.

Mean and periodic surface pressure distributions for this configuration have been extensively documented.[9,10] Surface pressure fluctuations measured using 6.25-mm condenser microphones, whose signals were amplified and digitized at 12,600 samples per second, corresponding to a 1-deg rotor phase resolution. No antialiasing filter was used since spectral analysis showed that the signal had negligible energy content beyond 4 kHz. The only filter in the circuit was the 10 kHz noise filter in the amplifier circuit. The data were sorted into 6-deg rotor phase intervals and averaged. Data digitized at 50,400 samples per second were used to check the effect of 1.5-deg phase resolution. Surface pressure spectra were also determined to study the nature of the boundary layer.

Flow Visualization

Vortex trajectories were determined using strobed laser-sheet visualization.[9] With the flow uniformly seeded with atomized mineral oil, vortex cores were seen as regions devoid of light-scattering particles. Videography was used to quantify the trajectories.

Velocity Measurements

Velocity measurements were made using a laser Doppler velocimeter (LDV). Being rotor-synchronized, the velocity components could be measured one at a time. Two components were measured, the streamwise U and the vertical V. Light was collected in backscatter, with a Field Stop module of 0.1 mm aperture used to minimize background scattering from surfaces normal to the optical axis. Velocity samples were collected in batches of 500 each. The data were sorted into 6-deg azimuth intervals, corresponding to a temporal resolution of 476 μs. Sixty such batches, totaling 30,000 values, were processed at each location. After sorting the 60th batch, the contents of each interval were averaged. Since this procedure consumed an average of 7 min for each measuring location, and the particle arrival rate was much lower in the core of the vortex than in other regions of the flowfield, measurements with finer phase resolution were not used. Inspection of the surface pressure data, presented later in this paper, indicate no reason to believe that details of the vortex core structure are being smeared out by the 6-deg averaging. It should be noted that any non-periodic fluctuations are smeared out by the averaging. The variance of the data in each interval was typically on the order of 1 m/s, but as the figures show, the mean was stable and varied smoothly from one interval to the next.

Results and Discussion

Vortex Trajectories

Figure 3 shows vortex trajectories reconstructed from visualization videotapes.[11] This figure looks at the cylinder from upstream. The vortex filaments are seen to move downward toward the cylinder. The downward motion is faster on the left-hand side of the figure because the induced velocity is higher under the advancing side of the rotor. Distortions are evident as the filaments reach the cylinder. Close to the surface, the visualization fails. As the vortex filaments interact with the cylinder, the seed particle deficit, which serves as the discriminant in the visualization, seems to disappear. Figure 4 shows the trajectories as viewed from above.[11] Here, the vortices move down as they move from left to right. Again, once the interaction occurs, the visualization fails.

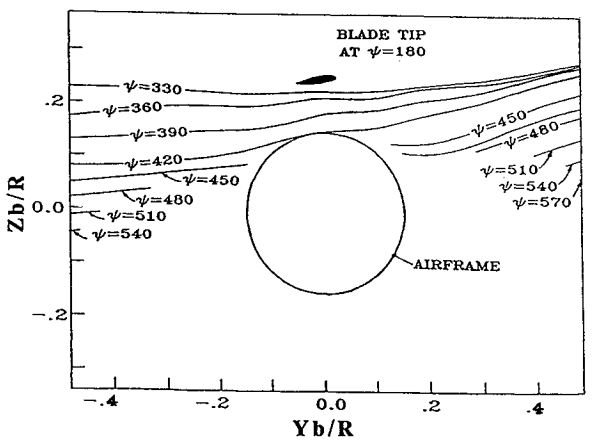

Fig. 3 Vortex trajectories viewed from upstream.

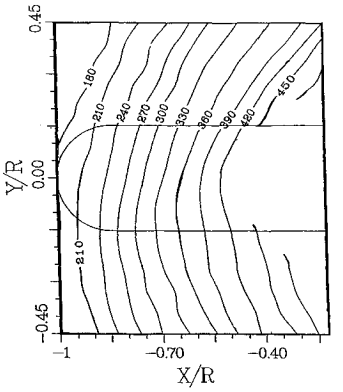

Fig. 4 Vortex trajectories viewed from above.

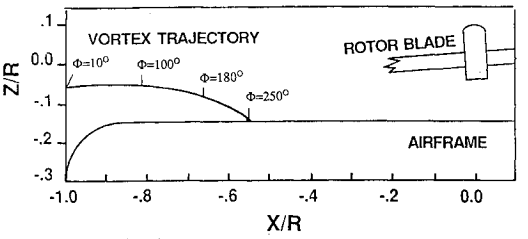

Fig. 5 Vortex trajectory in the vertical cross section through the cylinder axis.

The geometry of the vortex trajectories shows that along the top of the cylinder, the interaction is essentially a perpendicular one, where the axis of the filament is normal to the cylinder axis. Hence, this region was selected to perform initial studies of the interaction event. Later measurements showed that the velocity component along the vortex core is not negligible.[1] This will no doubt cause additional problems in modeling the interaction.

The vortex trajectory in the vertical cross section through the cylinder is shown in Fig. 5.[11] It is seen that the vortex core moves both downstream and downward. The approximate location and speed of motion of the core can be calculated from these data as functions of the rotor azimuth. One complication, not apparent from Fig. 5, is that as the blade passes this cross section, the vortex is pushed down faster.

Velocity Profiles and Vorticity Contours

A grid of measuring locations was set up in the vertical cross section through the cylinder axis, above the top of the airframe. The periodic variations of U and V were acquired at each node. Data obtained at specified rotor phase values were used to construct vorticity contours of the velocity field in the vertical plane, as shown in Figs. 6a and 6b. The tip vortex is seen as a strong region of positive vorticity (clockwise rotation). A region of negative vorticity appears under the tip vortex when it is well above the airframe. The present interpretation of this is that the boundary layer separates upstream due to the stagnation region induced by the vortex. Negative vorticity then appears above the vortex, and is seen to move rapidly and end up downstream of it. This is qualitatively con-

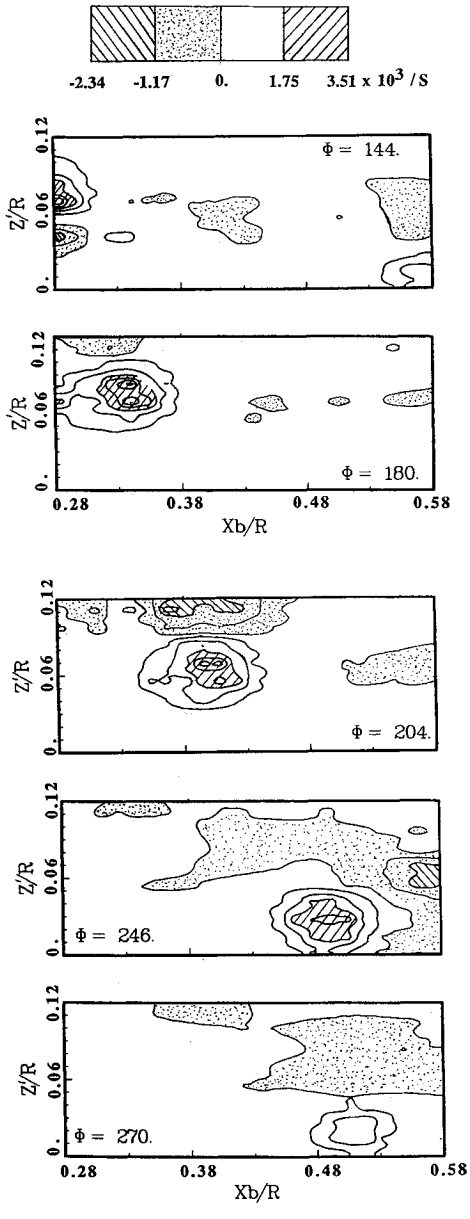

Fig. 6 Vorticity contours in the vertical cross section through the cylinder axis, as a function of rotor azimuth.

sistent with expectations from potential flow theory, due to the effects of the surface and the tip vortex on this "secondary vortex." However, this secondary structure may also be interpreted as being due to the inboard vortex sheet.

Both interpretations of the origin of the secondary structure are plausible. The velocity variation in the absence of the cylinder does not show multiple peaks as the vortex passes the measurement locations.[11] This would appear to support the boundary-layer argument. Vidotapes appear to show the vortex core getting flattened at the surface and then moving downstream. On the other hand, the observed pressure fluctuations can be explained qualitatively as the effects of the vortex sheet interacting with the surface.[10] The timing of these two events is such that the issue cannot yet be clearly resolved, but must await further experiments. The most likely explanation is that both effects occur.

The evolution of the vortex velocity profiles as the vortex descends toward the cylinder is summarized in Fig. 7. The figure shows the instantaneous U-component values along vertical lines above four stations on the top of the cylinder, marked 1–4. Each station represents the center of a microphone. The "instantaneous" profiles obtained at three different vortex ages ϕ are shown, from which the vortex core diameters can be discerned. The procedure was as follows: The LDV focal volume was successively positioned at 2.54-mm intervals of height above each station, and the data for the velocity component along the cylinder axis at each location were averaged in 6-deg rotor azimuth intervals. The data within the interval corresponding to a given azimuth were extracted from each output file, and vector plots were constructed after subtracting the freestream mean velocity (a constant for a given advance ratio) from the results. This was repeated for the three azimuth intervals shown.

At 162 deg, a distorted vortex profile can be seen above station 1 ($Xb/R = 0.284$). The distortion is partially due to the secondary structure, which rolls over the primary. At this time, the profiles above stations 2 ($Xb/R = 0.367$) and 3 ($Xb/R = 0.450$) show only weak induced velocity fields. The vortex center is 33 mm above the cylinder surface. The velocity immediately above the surface is equal and opposite to the freestream velocity, so that station 1 is approximately under a point of zero velocity, the stagnation being caused by the induced velocity field of the vortex. Obviously, this must have drastic effects on the boundary layer immediately upstream. At 204 deg, the vortex profile is identifiable above station 2, but its center is lower. The secondary vortex is now clearer, and is above the primary. At 246 deg, the vortex profile is above station 3, except that the bottom half of the profile has disappeared. At the same time, the velocity field above station 4 has changed substantially. It now has the form of another vortex, with a sense opposite to that of the original tip vortex. The secondary structure has completely separated from the

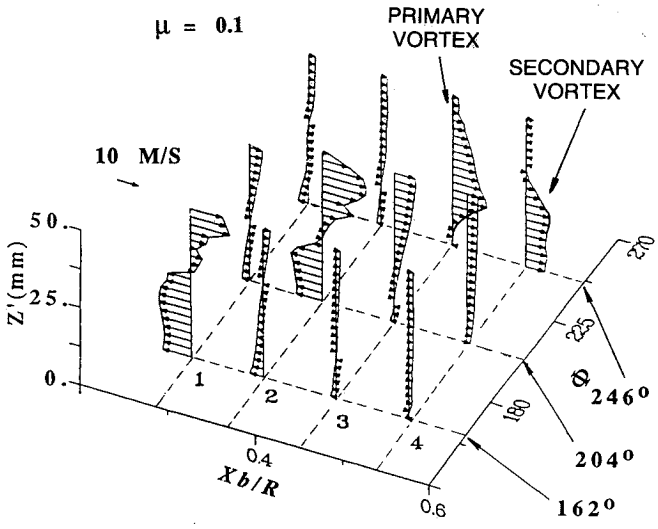

Fig. 7 Profiles of instantaneous ($U - U_\infty$) at three values of rotor azimuth above 4 stations along the top of the airframe.

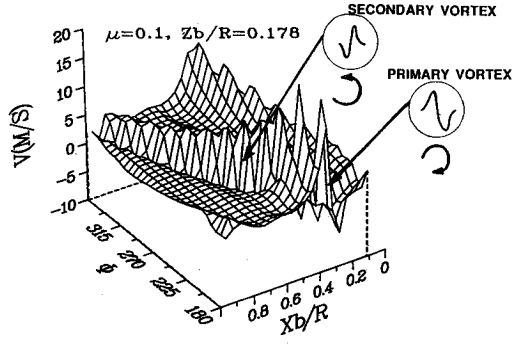

Fig. 8 Vertical velocity in a plane 12.5 mm above the top of the cylinder, as a function of rotor azimuth and distance along the airframe axis, showing the decay of the secondary vortex structure.

primary, and moves downstream as expected from image vortex considerations.

The subsequent decay of the secondary structure is evident from Fig. 8, which tracks the downward velocity at a fixed height of 12.5 mm above the top of the cylinder, as a function of downstream distance and vortex age. The vortex effect can be traced from the sequence of velocity variations along Xb/R. The sharp variation corresponding to the original tip vortex is first evident at about $Xb/R = 0.28$ (near station 1). The sequence here is shown in the inset circle marked "PRIMARY VORTEX," with the sense of vorticity sketched below. After the interaction (near $Xb/R = 0.45$), the velocity profile undergoes a sharp change: the sense of vorticity has reversed. This is marked "SECONDARY VORTEX." The subsequent convection of the secondary vortex is visible. The disturbance due to this feature decays rapidly, becoming quite small by $Xb/R = 0.9$.

Surface Pressure Variations

The nature of the boundary layer upstream of the interaction location was examined by measuring the autospectrum of a microphone signal. The boundary layer was seen to have significant broadband pressure fluctuation energy going well past 2000 Hz. It may be assumed therefore that the upstream boundary layer is turbulent.

Figure 9 shows periodic pressure variations at station 2. The peaks at 180 and 360 deg of rotor azimuth in Fig. 9a correspond to the passage of the rotor blades. The secondary peaks at around 22 and 202 deg are caused by the tip vortex. One issue is whether there are additional details to be captured by going to higher temporal resolution as the vortex passes over. This is studied in Fig. 9b, where the 60 available slots are distributed over the first 90 deg of azimuth. The periodic variation is quite smooth, and no additional details appear. The pressure signature is not symmetric with respect to the vortex center, for several possible reasons. First, the tip vortex structure is distorting. Second, the boundary layer may be separating. Third, there is the vortex sheet nearby. The precise cause cannot be isolated from these data.

To see whether details were being lost by averaging the data over many cycles of rotor revolution, some of these averaged results were compared with the results obtained during just one rotor revolution.[12] The two sets of data were essentially identical. Minor variations in amplitude were observed at the pressure peaks during vortex passage, but no additional details appeared. Only averaged data are presented here.

A curious feature of the flowfield is seen in Fig. 10a, which shows pressure variations over station 3. Here, the blade passage peaks are minor compared to the effects of vortex passage, but are repeatable. However, the vortex passages are certainly not repeatable from one blade to the next. This phenomenon was studied by observing the pressure signature on an oscilloscope during the data acquisition. The surprising observation was that the waveform remained the same from one cycle of the rotor to the next, and varied, if at all, quite slowly. The discrepancy must be attributed to some minor difference between the two blades. The details of the first vortex are shown in Fig. 10b. No secondary features are seen even during close passage of the core. The pressure trace is not symmetric about its minimum.

Figures 11–13 compare the azimuth-resolved velocity variations 12.5 mm above the microphone locations to the surface pressure measured by the microphones. The locations were chosen to see the nature of these variations before, during, and after the vortex-surface interaction. The approximate times of occurrence of major events are marked on the figures. The blade passage occurs at 0 and 180 deg. In Fig. 11, the microphone is located upstream of where the tip vortex impinges on the surface. The tip vortex passes over the microphone (at $Xb/R = 0.367$) soon after the blade passage. The U component of velocity decreases sharply and goes negative as the vortex passes. The V component changes direction from being downwards before the vortex center passes, to being upwards afterwards. The passage of the blade causes a sharp increase in the unsteady pressure. As U decreases to zero, the pressure should reach a positive peak, but this peak is lost in the trace corresponding to blade passage. The pressure reaches a minimum when U reaches its highest negative value, and then rises to a peak when U again crosses zero. Figure 12 shows data at $Xb/R = 0.534$, where the tip vortex and the secondary vortex are still present. Thus, both effects are seen. There is no reversal of U in this figure, although the V

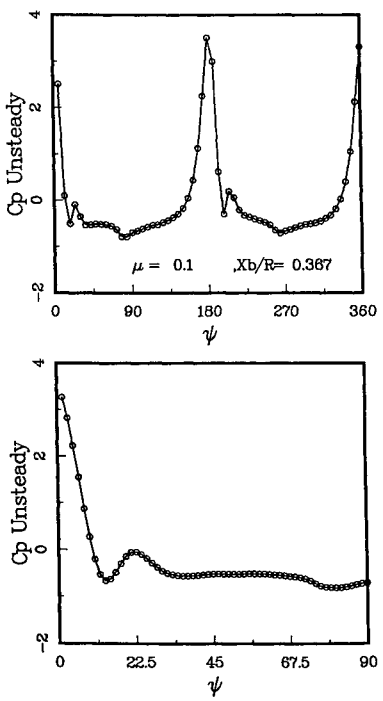

Fig. 9 Phase-averaged pressure variation at microphone station 2 over one complete revolution and during the 90 deg including vortex passage.

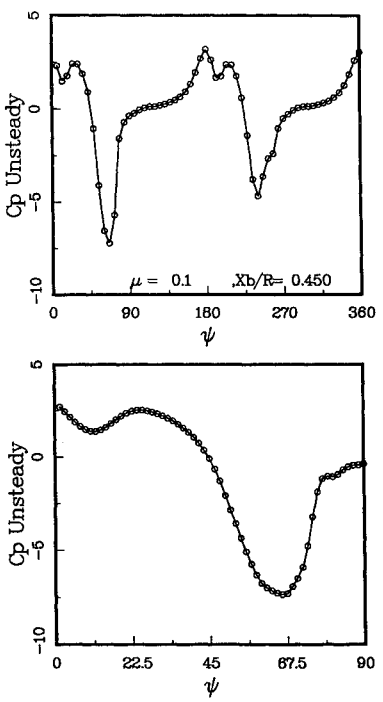

Fig. 10 Phase-averaged pressure variation at microphone station 3 over one complete revolution and during the 90 deg including vortex passage.

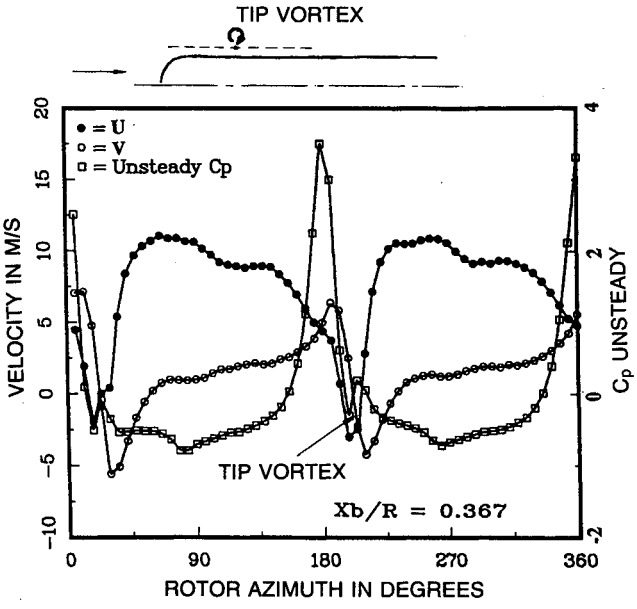

Fig. 11 Comparison of phase-averaged surface pressure variation at station 2 with the velocity variation 12.5 mm above it.

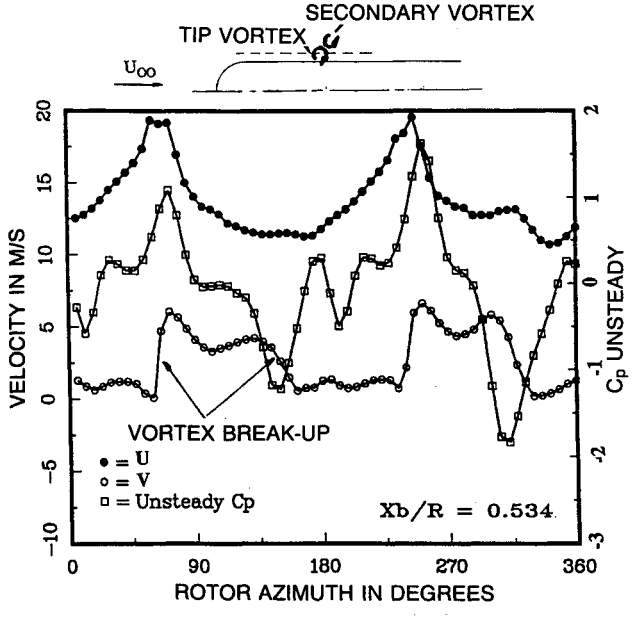

Fig. 12 Comparison of phase-averaged surface pressure variation at station 4 with the velocity variation 12.5 mm above it.

component still shows a vortex signature, since the bottom half of the primary vortex no longer exists as an organized flow. The secondary vortex is still above the surface. One feature of this figure is the simultaneous occurrence of high pressure and high streamwise velocity, during the interaction of the primary vortex with the surface. The rotor tip vortex originates from the boundary layer around the tip of the blade, which moves very rapidly relative to the freestream. If this flow is stopped at the cylinder surface, the resulting stagnation pressure will be close to that at the leading edge of the rotor blade, much higher than the stagnation pressure at the nose of the cylinder. This effect has been confirmed both using the pressure distribution on the cylinder, and by direct measurement of the stagnation pressure variation across the wake.[10] As the secondary vortex passes, the pressure decreases to a minimum, which is consistent with the anticlockwise sense of rotation of this structure. Data at $Xb/R = 0.617$ are shown in Fig. 13. Here, only the secondary vortex remains, rotating counterclockwise. Thus, the observed effects are reversed in sense from those due to the tip vortex. The range of variation of pressure is considerably lower than in Fig. 12, since the vortex structures are dissipating.

Comparison of Vortex Behavior with Two-Dimensional Potential Flow Concepts

The strength of the tip vortex was calculated using the peak circulatory velocity obtained from the profiles across the vortex, and was used to estimate induced velocities. This is a rather crude calculation: the flowfield outside this region is not really irrotational, and a doubling of the radius for this calculation would have produced a 10% increase in measured vortex strength. Thus, the circulation was obtained as

$$\Gamma = 2\pi * r_0 * V_{max}$$

where r_0 is the radius of the vortex core as defined by the peak circulatory velocity V_{max}. For example, at $Xb/R = 0.284$ and rotor phase of 162 deg, the circulation strength Γ was 1.508 m^2/s. Some calculations have been performed to compare the measured deflections and induced velocities with predictions made using two-dimensional geometry and potential flow con-

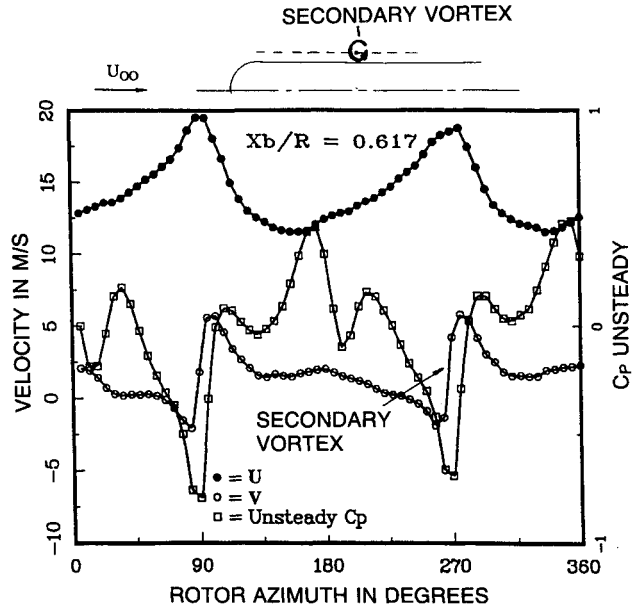

Fig. 13 Comparison of phase-averaged surface pressure variation at $Xb/R = 0.617$ with the velocity variation 12.5 mm above it.

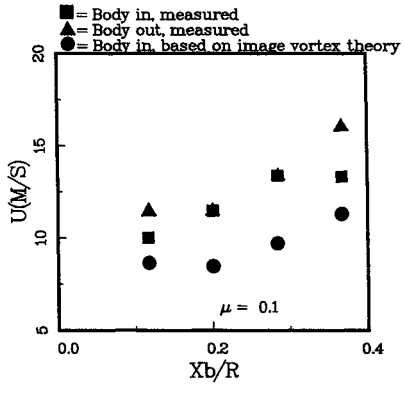

Fig. 14 Comparison of measured streamwise velocity with the cylinder present and absent, with the velocity calculated using two-dimensional potential flow theory based on "image vortex" concepts.

cepts. The deflections due to the cylinder were defined as differences between data obtained with and without the cylinder present. The results are shown in Fig. 14, where the U component of the convection velocity of the tip vortex is show as a function of distance along the cylinder axis. The "body out, measured" data are used as the baseline data set. The actual velocity measured with the body in are compared with the velocity calculated assuming that the body behaves as a flat plate in potential flow. The results indicate qualitative agreement, but the quantitative error is quite large. It must be noted that the phenomena are even more complex on the sides of the cylinder, and the viscous effects during core interaction will be much more pronounced there. Reference 13 presents evidence that potential flow calculations of vortex deflection disagree with measured pressure variations on the port side of the cylinder. This side is inaccessible to the LDV at present.

Conclusions

The transient, periodic interaction of a helical vortex with a cylinder has been studied experimentally. The interaction process appears to involve the creation and convection of secondary vortical structures. Several of the effects at the surface appear to be due to these secondary structures. The following may be stated in conclusion.

1) Close approach of the tip vortex causes stagnation and flow reversal near the surface.

2) Regions of negative vorticity are created under the tip vortex when it is still well above the surface. Later, such a region appears above the vortex, and moves rapidly downstream.

3) As the primary structure impacts the surface, its lower part disappears. A secondary structure simultaneously appears downstream.

4) The secondary structure moves rapidly downstream, but rapidly dissipates.

5) The surface pressure variation corresponds to the structure of the tip vortex until the vortex impinges on the surface. Thereafter, the pressure trace is dominated by the secondary vortex structure. Simultaneous peaks in velocity and surface pressure are seen, due to the high stagnation pressure in the tip vortex.

6) Vortex deformations and induced velocities do not agree quantitatively with two-dimensional potential theory at the top of the airframe, even before the vortex impinges on the surface.

Acknowledgments

This work was supported by the U.S. Army Research Office under Contract DAAG29-82-K-0084, the Center of Excellence in Rotary Wing Aircraft Technology. Thomas Doligalski is the technical monitor. The authors are also grateful to Albert Brand, who performed the flow visualization.

References

[1]Komerath, N. M., Liou, S. G., Brand, A. G., and McMahon, H. M., "A Study of the Encounter Between a Helical Vortex and a Circular Cylinder," AIAA Paper 88-2622, July 1988.

[2]Stremel, P. M., "Aerodynamic Interaction Between Vortical Wakes and the Viscous Flow about a Circular Cylinder," AIAA Paper 85-4063, Oct. 1985.

[3]Harvey, J. K., and Perry, F. J., "Flowfield Produced by Trailing Vortices in the Vicinity of Ground," *AIAA Journal,* Vol. 9, Aug. 1971, pp. 1659–1660.

[4]Atiahs, M., and Weihs, D., "Motion of Trailing Vortices near the Ground," *Journal of Aircraft,* Vol. 21, Oct. 1984, pp. 783–786.

[5]Doligalski, T. L., and Walker, J. D. A., "The Boundary Layer Induced by a Convected Two-Dimensional Vortex," *Journal of Fluid Mechanics,* Vol. 139, Feb. 1984, pp. 1–28.

[6]Walker, J. D. A., Smith, C. R., Cerra, A. W., and Doligalski, T. L., "The Impact of a Vortex Ring on a Wall," *Journal of Fluid Mechanics,* Vol. 181, 1987, pp. 99–140.

[7]Simons, I. A., Pacifico, R. R., and Jones, J. P., "The Movement, Structure, and Breakdown of Trailing Vortices from a Rotor Blade," *Proceedings of the CAL/USAA AVLABS Symposium,* Buffalo, NY, June 1966.

[8]Bliss, D. B., "Treatment of Vortex/Surface Interactions for Rotorcraft Interactional Aerodynamics," *Proceedings of the ARO Interactional Helicopter Aerodynamics Workshop,* U.S. Army Research Office, Durham, NC, July 7, 1988.

[9]Brand, A. G., Komerath, N. M., and McMahon, H. M., "Results from the Laser-Sheet Visualization of an Incompressible Vortex Wake," *Journal of Aircraft,* Vol. 26, May 1989, pp. 438–443.

[10]Brand, A. G., "An Experimental Investigation of the Interaction Between a Model Rotor and Airframe in Forward Flight," Ph.D. Thesis, Georgia Inst. of Technology, School of Aerospace Engineering, Atlanta, GA, March 1989, pp. 162–163.

[11]Liou, S. G., Komerath, N. M., and McMahon, H. M., "The Velocity Field of a Circular Cylinder in the Wake of a Rotor in Forward Flight," *Journal of Aircraft* (to be published).

[12]Liou, S. G., "Velocity Measurements on a Lifting Rotor/Airframe Configuration in Low-Speed Forward Flight," Ph.D. Thesis, Georgia Inst. of Technology, School of Aerospace Engineering, Atlanta, GA, Dec. 1988.

[13]Mavris, D. M., "An Analytical Method for the Prediction of Rotor/Airframe Aerodynamic Interactions," Ph.D. Thesis, Georgia Inst. of Technology, School of Aerospace Engineering, Atlanta, GA, Dec. 1988.